Dyes and Pigments 89 (2011) 9–15

Contents lists available at ScienceDirect

Dyes and Pigments

journal homepage: www.elsevier.com/locate/dyepig

Synthesis and fluorescent characteristics of imidazole–indocyanine green conjugates

Christopher Pavlik [a], Nrusingh C. Biswal [b], Faith Corbo Gaenzler [a], Martha D. Morton [a], Liisa T. Kuhn [c], Kevin P. Claffey [d], Quing Zhu [b], Michael B. Smith [a,*]

[a] Department of Chemistry, University of Connecticut, 55 N. Eagleville Road, Storrs, CT 06269-3060, USA
[b] Department of Electrical and Computer Engineering, University of Connecticut, 371 Fairfield Way, Storrs, CT 06269-2157, USA
[c] Department of Reconstructive Sciences, MC1615, University of Connecticut Health Center, 263 Farmington Avenue, Farmington, CT 06030-1615, USA
[d] Department of Cell Biology, University of Connecticut Health Center, 263 Farmington Avenue, Farmington, CT 06032, USA

ARTICLE INFO

Article history:
Received 5 May 2010
Received in revised form
11 August 2010
Accepted 16 August 2010
Available online 31 August 2010

Keywords:
Nitroimidazole
Indocyanine green
Fluorescence
Near infrared
Dye
Hypoxia

ABSTRACT

We have successfully synthesized imidazole-dye conjugates by linking imidazole and nitroimidazoleacetic acids to an indocyanine green (ICG) carboxylic acid derivative, using an ethanolamine linker. These dye-conjugates show absorbance peaks at 754–756 nm and fluorescence peaks at 780 nm. The dye-conjugates show a blue shift of 25 nm and 30 nm in the absorption and fluorescence spectra respectively when compared to that of standard cardiogreen. There is no change in absorption and fluorescence spectral profiles between the ICG derivative and imidazole conjugates. The extinction coefficients of new ICG derivative and imidazole conjugates are 1.8 times higher than that of standard ICG. The relative quantum yields of the new compounds are 4.5–5.5 times higher than that of the Sigma–Aldrich's ICG. The dyes are tested for hypoxia *in-vitro* with 4T1 luc cell lines and it is found that the cells treated with 2-nitroimidazole ICG show a contrast of fluorescence signal of 2.5–3.0 for the cells under hypoxic to that of cells under normoxic. However pure ICG shows no significant difference between hypoxic and normoxic cells.

1. Introduction

Most cancerous solid tumours contain a tumour-specific microenvironment that is characterized by low oxygen partial pressure (PO2) and low pH [1]. The tumour microenvironment is recognized as a critical factor that influences not only the response to conventional anti-cancer therapies, but also helps define the potential for malignant progression and metastasis [2]. An inadequate supply of nutrients and oxygen to the tumour regions causes tumour tissue hypoxia. It is known that tumour hypoxia alters the pattern of gene expression, leading to more aggressive behavior with increased metastatic potential and treatment resistance. Tumour hypoxia is an important indicator of tumour metabolism and tumour response to various forms of therapy. Currently, the PO2 measurements in human tumours *in-vivo* have been performed using invasive polarographic needle electrodes. However, the use of electrodes is only suitable for measuring PO2 in superficial tumours, such as cervix [3] and head and neck [4]. Non-invasive methods such as Magnetic Resonance Imaging (MRI), and Positron emission tomography (PET) have been used to image tumour hypoxia probes [5]. However, both MRI and PET systems are expensive for routine clinical use in longitudinal imaging assessments over the course of neoadjuvant chemotherapy. Therefore, it is important to develop a non-invasive, low cost method to repeatedly monitor changes related to hypoxia.

Fluorescence imaging is an optical imaging technique that is useful tool for diagnostic imaging without the complications that often accompany the use of nuclear contrast agents[6]. The fluorescence imaging systems are cost effective and highly portable. In fluorescence imaging, a near-infrared (NIR) fluorescent probe (>700 nm) is administered, and irradiation with NIR light allows collection of the remitted fluorescence for imaging. Fluorescence imaging has a tremendous potential for probing tumour molecular markers associated with tumour proliferation, growth, and metastasis. To the best of our knowledge, there are no hypoxia probes capable of real-time fluorescence imaging of tumour hypoxia in the NIR spectrum.

Indocyanine dyes are important abiotic molecules [7–10], and useful NIR probes. An important member of this family is the clinically approved indocyanine green (ICG, **1**), which has many

* Corresponding author. Tel.: +1 860 486 2881; fax: +1 860 486 2981.
E-mail address: michael.smith@uconn.edu (M.B. Smith).

0143-7208/$ – see front matter © 2010 Elsevier Ltd. All rights reserved.
doi:10.1016/j.dyepig.2010.08.008

applications for fluorescence imaging [11,19]. ICG is the only FDA approved agent that can be used for human subjects, due to the very low toxicity and high absorbance in the NIR spectrum. The use of ICG in molecular imaging probes may be limited because it loses its fluorescence after protein binding. However, a NIR probe is available after cell binding and internalization, due to the fact that ICG may be dissociated from the targeting antibody, thus activating fluorescence [12]. It is known, for example, that ICG binds to plasma proteins, and protein-bound ICG emits light with a peak wavelength of about 830 nm in the NIR [13]. Based on this knowledge, intravenous injection of ICG was used to delineate hepatocellular carcinoma during open hepatectomy [14]. Further, laparoscopic fluorescent imaging using preoperative injection of ICG enabled real-time identification of hepatocellular carcinoma [15]. A final example is the report of sentinel node mapping guided by ICG fluorescence imaging in gastrointestinal cancer [16]. Hydrophilic cyanine dyes have been used for tumour imaging in the NIR [17]. Despite these applications of ICG, there are several limitations, including optical instability in body, low quantum yield, and promiscuous leakage in blood vessels. Our approach will advance fluorescence imaging by providing methodology to image tumour hypoxia in addition to tumour vasculature. We now report the preparation and testing of new synthetic contrast agents, referred to here as dye-conjugates, to enhance the sensitivity and specificity of near-infrared (NIR) imaging in the detection of tumour hypoxia [13,18,19]. These novel dye-conjugates link a 2-nitroimidazole moiety with known hypoxia marker properties to an ICG derivative.

2. Materials and methods

All reagents and chemicals were used as received from Aldrich or Acros and used without further purification. All glassware was flame-dried under vacuum, and all reactions were performed under a nitrogen atmosphere, unless otherwise noted. All solvents were dried according to standard procedures. Thin-layer chromatography was done on Fluka aluminum-backed TLC plates with fluorescent indicator and 0.2 mm silica gel layer thickness, and *p*-anisaldehyde in methanol was used as a developing agent. Column chromatography was done using 60 Å porosity, 32–63 μm silica gel and 90 Å porosity, 32–63 μm C_{18}-reverse phase silica gel. An HP Model 5970B GC/MSD with an HP-1 column Gas chromatogram/mass spectrometer was used for GC/MS spectra. The ^{1}H, ^{13}C, and 2D-COSY NMR were collected on a Brüker Avance 300 (300.13 MHZ ^{1}H, 75.48 MHZ ^{13}C). Chemical shifts are reported in ppm (δ) downfield from TMS, in $CHCl_3$, unless otherwise noted.

2.1. 2,3,3-Trimethyl-3H-indole-5-carboxylic acid, **6**

A mixture of 4-hydrazinobenzoic acid (**5**, 4.56 g, 30.0 mmol), 3-methylbutan-2-one (3.70 g, 42.0 mmol) and sodium acetate (4.92 g, 60.0 mmol) was stirred in glacial acetic acid (50 mL) for 1 h then heated at reflux overnight. After removal of the acetic acid *in vacuo*, 10% MeOH (80 mL) was added to the residue and the resulting precipitate was filtered and dried to yield **6** (5.36 g, 26.37 mmol, 88%) of as a tan solid [20]. ^{1}H NMR: δ 8.12 (dd, 1H, 8 Hz), 8.04 (s, 1H), 7.60 (d, 1H, $J = 8$ Hz), 2.36 (s, 3H), 1.35 (s, 6H); ^{13}C NMR: δ 192.9, 171.4, 156.8, 145.8, 131.0, 128.4, 123.4, 120.0, 54.3, 23.0, 15.6.

2.2. 5-Carboxy-1-(δ-sulfobutyl)-2,3,3-trimethyl-3H-indolium betaine, **7**

A mixture of **6** (1.00 g, 4.92 mmol) and 1,4-butanesultone (2.93 mL, 28.68 mmol) was heated at reflux overnight in 1,2-dichlorobenzene (20 mL). A red precipitate was formed, filtered, rinsed with acetone and dried to give 1.54 g (4.52 mmol, 92%) of **7** as a red solid. ^{1}H NMR (MeOD): δ 8.44 (s, 1H), 8.32 (dd, 1H, $J = 1.4$, 8.2 Hz), 8.15 (d, 1H, $J = 8.8$ Hz), 4.63 (t, 2H, $J = 7.5$ Hz), 4.43 (s, 3H), 2.86 (t, 2H, $J = 7.1$ Hz), 2.16 (m, 2H), 1.97 (m, 2H), 1.70 (s, 6H); ^{13}C NMR (DMSO): δ 197.8, 168.1, 148.3, 144.0, 127.7, 127.5, 126.8, 51.1, 49.3, 42.1, 27.3, 26.7, 9.8 [20].

2.3. Bis-1,1′-(4-sulfobutyl)indoletricarbocyanine-5,5′-dicarboxylic acid sodium salt, **9**

A mixture of **7** (5 g, 14.5 mmol) and *N*-((1*E*,3*E*)-5-(phenylimino) penta-1,3-dienyl)benzenamine (**8**, 2 g, 7 mmol) was added to acetic anhydride (75 mL) and glacial acetic acid (45 mL). Sodium acetate (2.05 g, 25 mmol) was added to this suspension, with vigorous stirring, and the reaction mixture was heated at reflux for 45 min. Upon cooling to ambient temperature the mixture was poured into 250 mL of hot anhydrous ether. Upon cooling, a precipitate formed and was collected via vacuum filtration and then washed with ether. The solid was recrystallized from H_2O/propanol (1:4) after standing at ~5 °C overnight. The crystals were collected by vacuum filtration and washed with cold propanol and allowed to dry for two days under vacuum to yield **9** (4.5 g, 5.73 mmol, 85% yield) [17]. ^{1}H NMR (DMSO): δ 12.98 (s, 2H) 8.08 (d, 2H, $J = 1.2$ Hz), 7.98 (dd, 2H, $J = 1.1$, 8.2 Hz), 7.95 (m, 5H), 7.51 (d, 2H, $J = 8.7$ Hz), 6.65 (t, 2H, $J = 12.4$ Hz), 6.54 (d, 2H, $J = 13.6$ Hz), 4.11 (m, 4H), 3.09 (m, 4H), 1.75 (m, 8H), 1.67 (m, 12H). ^{13}C NMR (DMSO): δ 206.5, 172.2, 166.9, 148.9–145.9, 145.8, 141.1, 130.6, 126.7, 123.2, 110.9, 105.0, 50.7, 48.4, 43.7, 40.1, 30.7, 27.0, 26.0, 22.4.

2.4. Methyl 2-(1H-imidazol-1-yl)acetate, **10a**

Imidazole (0.60 g, 8.85 mmol) was added to a mixture of methyl bromoacetate (0.84 mL, 8.85 mmol), potassium carbonate (1.8 g, 13.27 mmol), and tetrabutylammonium iodide (TBAI) (0.070 g, 0.185 mmol) in 10 mL of acetonitrile. The mixture was heated to 80 °C and stirred vigorously at this temperature for 40 min. After cooling to ambient temperature, the inorganic salts were removed by vacuum filtration and washed with acetonitrile. The filtrate and washings were combined and the solvents evaporated *in vacuo* to yield a residue that was recrystallized from ethyl acetate and petroleum either (50:1) to give **10a** [21,22] (1.14 g, 8.05 mmol, 91%). Mp, 55–56 °C. ^{1}H NMR (DMSO): δ 7.38 (s, 1H), 7.19(s, 1H) 7.1 (s, 1H), 5.18 (s, 2H); 3.73 (s, 3H); ^{13}C NMR (DMSO): δ 170.0, 137.8, 126.7, 120.3, 54.7, 46.8.

2.5. Methyl 2-(4-nitro-1H-imidazol-1-yl)acetate, **10b**

4-Nitroimidazole (1 g, 8.85 mmol) was added to a mixture of methyl bromoacetate (0.84 mL, 8.85 mmol), potassium carbonate (1.8 g, 13.27 mmol), and TBAI (0.070 g, 0.185 mmol) in 10 mL of acetonitrile. The mixture was heated to 80 °C, and stirred vigorously at this temperature for 40 min. After cooling the ambient temperature, the inorganic salts were removed by vacuum filtration and washed with acetonitrile. The filtrate and washings were combined and the solvents evaporated *in vacuo* to give a residue that was recrystallized from ethyl acetate to yield **10b** [23] (1.46 g, 7.87 mmol, 89%). Mp, 129–130 °C. ^{1}H NMR (DMSO): δ 8.37 (s, 1H), 7.82 (s, 1H), 5.10 (s, 1H); ^{13}C NMR (DMSO): δ 168.5, 147.3, 138.8, 123.0, 53.0, 48.7.

2.6. Methyl 2-(2-nitro-1H-imidazol-1-yl)acetate, **10c**

2-Nitroimidazole (1 g, 8.85 mmol) was added to a mixture of methyl bromoacetate (0.84 mL, 8.85 mmol), potassium carbonate (1.8 g, 13.27 mmol), and TBAI (0.070 g, 0.185 mmol) in 10 mL of acetonitrile. The mixture was heated to 80 °C and stirred vigorously

at this temperature for 40 min. After cooling the to room temperature, the inorganic salts were removed by vacuum filtration and washed with acetonitrile. The filtrate and washings were combined and the solvents were evaporated *in vacuo* to give a residue that was recrystallized from ethyl acetate to yield **10c** [24,25] (1.32 g, 7.16 mmol, 81%). Mp, 95–96 °C. ^{1}H NMR: δ 7.11 (s, 1H), 7.05 (s, 1H), 5.09 (s, 2H), 3.77 (s, 3H); ^{13}C NMR: δ 166.5, 126.5, 127.3, 53.2, 50.7.

2.7. N-(2-Hydroxyethyl)-2-(1H-imidazol-1-yl)acetamide, **11a**

Methyl 2-(1H-imidazol-1-yl)acetate, **10a** (0.48 g, 3.39 mmol), was added to 6 mL of absolute MeOH. The solution was vigorously stirred while freshly distilled aminoethanol (0.90 mL, 13.59 mmol) was added slowly, and the reaction was stirred overnight at ambient temperature [26]. The reaction mixture was then concentrated and the remaining solid was dissolved in dry acetone and passed through a plug of silica. The resulting residue was recrystallized from ethyl acetate to yield **11a** (0.396 g, 2.34 mmol, 69%). Mp, 132.8–134.0 °C. ^{1}H NMR (MeOD): δ 7.70 (s, 1H) 7.14 (s, 1H), 7.01 (s, 1H), 4.74 (s, 2H), 3.63 (t, 2H, J = 5.7 Hz), 3.43 (t, 2H, J = 5.7 Hz, MeOD overlap); ^{13}C NMR (MeOD): δ 168.1, 138.1, 127.6, 120.3 59.9, 41.8. HR-TOF MS. Calcd for $C_7H_{11}N_3O_2Na$ ($M + Na^+$), m/z 192.0649. Found, m/z 192.0673.

2.8. N-(2-Hydroxyethyl)-2-(4-nitro-1H-imidazol-1-yl)acetamide, **11b**

Methyl 2-(4-nitro-1H-imidazol-1-yl)acetate, **10b** (0.636 g, 3.39 mmol), was added to 6 mL of absolute MeOH. The solution was vigorously stirred while freshly distilled aminoethanol (0.90 mL, 13.59 mmol) was added slowly, and the reaction was stirred overnight at ambient temperature [26]. The reaction mixture was concentrated and the resulting solid was recrystallized from ethyl acetate to yield **11b** (0.587 g, 2.74 mmol, 81%). Mp, 136–137 °C. ^{1}H NMR (MeOD): δ 8.32 (s, 1H) 8.17 (s, 1H), 7.74 (s, 1H), 4.90 (s, 2H), 4.71 (s, 1H,), 3.62 (t, 2H, J = 5.7 Hz), 3.38 (t, 2H, J = 5.7 Hz); ^{13}C NMR (MeOD): δ 172.1, 137.8, 121.33, 59.9, 49.4, 41.8. HR-TOF MS. Calcd for $C_7H_{10}N_4O_4Na$ ($M + Na^+$), m/z 1237.0600. Found, m/z 237.0636.

2.9. N-(2-Hydroxyethyl)-2-(2-nitro-1H-imidazol-1-yl)acetamide, **11c**

Methyl 2-(2-nitro-1H-imidazol-1-yl)acetate, **10c** (0.636 g, 3.39 mmol), was added to 6 mL of absolute MeOH. The solution was vigorously stirred while freshly distilled aminoethanol (0.90 mL, 13.59 mmol) was added slowly, and the reaction was stirred overnight at ambient temperature [26]. The reaction mixture was concentrated and the remaining solid was dissolved in dry acetone and passed through a plug of silica. The resulting residue was recrystallized from ethyl acetate to give **11c** [27] (0.587 g, 2.74 mmol, 81%). Mp, 163.5–164.7 °C. ^{1}H NMR (MeOD): δ 7.52 (s, 1H), 7.37 (d, 1H, J = 0.9 Hz), 5.36 (s, 2H), 3.85 (t, 2H, J = 5.4 Hz), 3.58 (t, 2H, J = 5.6 Hz); ^{13}C NMR (MeOD): δ 166.1, 156.3127.5, 127.3, 60.1, 51.4, 41.8.

2.10. N-(2-Hydroxyethyl)-2-(1H-imidazol-1-yl)acetamido-ICG, **12a**

ICG derivative **9** (0.162 g, 0.216 mmol) was dissolved in 2.49 mL of DMF. This solution was treated with a catalytic amount of DMAP, and the solution was cooled to 0 °C. DCC (0.094 g, 0.454 mmol) was added, and the mixture was stirred for 30 min [17,28]. Addition of **11a** (0.167 g, 0.990 mmol) was followed by stirring for 2 h at 0 °C, warming to ambient temperature and then stirring overnight. The reaction mixture was concentrate and poured into 25 mL of anhydrous ether, and the resulting precipitate was collected. Column chromatography on C_{18}-reverse phase silica using H_2O/MeOH (1:1.1–1:1) gave **12a** (0.102 g, 0.0864 mmol, 40%). NMR (DMSO): δ 7.81 (d, J = 1.3 Hz, 1H), 7.75–7.41 (m, 12H), 7.09 (s, 1H), 6.88 (s, 1H), 6.7 (t, J = 12.2 Hz, 2H), 6.60 (d, J = 13.2 Hz, 2H), 4.7 (s, 2H), 4.52 (t, J = 5.4 Hz, 2H), 4.2–4.01 (m, 4H), 3.61 (t, J = 5.3 Hz, 2H), 3.0 (m, 4H), 1.91–1.70 (m, 8H), 1.70–1.57 (m, 12H); ^{13}C NMR (DMSO): δ 206.8, 172.1, 168.0, 167.6, 166.3, 159.7, 148.9–144.9, 144.8, 141.0, 138.1, 130.8, 129.7, 128.3, 127.7, 123.4, 120.2, 110.5, 105.1, 49.8, 44.0, 30.4, 29.8, 27.9, 26.8, 22.4. HR-TOF MS. Calcd for $C_{51}H_{61}N_8O_{12}S_2Na_2$ ($M + Na^+$), m/z 1087.3646. Found, m/z 1087.3641.

2.11. N-(2-Hydroxyethyl)-2-(4-nitro-1H-imidazol-1-yl)acetamido-ICG, **12b**

ICG derivative **9** (0.162 g, 0.216 mmol) was dissolved in 2.49 mL of DMF. This solution was treated with a catalytic amount of DMAP, and the solution was cooled to 0 °C. DCC (0.094 g, 0.454 mmol) was added, and the mixture was stirred for 30 min [17,28]. Addition of **11b** (0.212 g, 0.990 mmol) was followed by stirring for 2 h at 0 °C, warming to ambient temperature and then stirring overnight. The reaction mixture was concentrate and poured into 25 mL of anhydrous ether, and the resulting precipitate was collected. Column chromatography on C_{18}-reverse phase silica using H_2O/MeOH (1:1.1–1:1) gave **12b** (0.142 g, 0.121 mmol, 56%). ^{1}H NMR (DMSO): δ 8.13 (s, 1H), 7.82 (d, J = 1.3 Hz, 2H), 7.79–7.30 (m, 1H), 6.64 (t, J = 12.3 Hz, 2H), 6.53 (d, J = 13.2 Hz, 2H), 4.68 (s, 2H), 4.07 (t, J = 5.7 Hz, 2H), 4.10 (m, 4H), 3.64 (t, J = 5.7 Hz, 2H), 3.05 (m, 4H), 1.87–1.70 (m, 8H), 1.70–1.56 (m, 12H); ^{13}C NMR (DMSO): δ 204.4, 172.8, 172.1, 168.3, 166.7, 164.8, 152.5, 149.3–146.1, 146.0, 140.9, 138.1, 130.7, 137.9, 136.8, 133.2, 121.0, 110.6, 114.9, 62.7, 49.2, 47.0, 44.3, 34.5, 30.2, 28.3, 27.1, 22.4. HR-TOF MS. Calcd for $C_{51}H_{59}N_{10}O_{16}S_2Na_2$ ($M + Na^+$), m/z 1177.3347. Found, m/z 1117.3341.

2.12. N-(2-Hydroxyethyl)-2-(2-nitro-1H-imidazol-1-yl)acetamido-ICG, **12c**

ICG derivative **9** (0.162 g, 0.216 mmol) was dissolved in 2.49 mL of DMF. To this solution was added a catalytic amount of DMAP and the solution was cooled to 0 °C. DCC (0.094 g, 0.454 mmol) was added, and the mixture was allowed to stir for 30 min [17,28]. Addition of **11c** (0.212 g, 0.990 mmol) was followed by stirring for 2 h at 0 °C, warming to ambient temperature and then stirring overnight. The reaction mixture was concentrate and poured into 25 mL of anhydrous ether, and the resulting precipitate was collected. Column chromatography on C_{18}-reverse phase silica using H_2O/MeOH (1:1.1–1:1) gave **12c** (0.112 g, 0.095 mmol, 44%). ^{1}H NMR (DMSO): δ 7.83 (d, J = 1.2 Hz, 2H), 7.8–7.5 (m, 7H), 7.45 (d, J = 8.5 Hz, 2H), 7.36 (s, 1H), 6.65 (t, J = 12.5 Hz, 2H), 6.53 (d, J = 13.3 Hz, 2H), 4.69 (s, 2H), 4.51 (t, J = 5.3 Hz, 2H), 4.2–4.0 (m, 4H), 3.65 (t, J = 5.6 Hz, 2H), 3.04 (m, 4H), 1.92–1.70 (m, 8H), 1.70–1.55 (m, 12H); ^{13}C NMR (DMSO): δ 202.3, 171.4, 167.5, 166.8, 166.0, 146.7, 144.0, 143.9–140.8, 140.7, 140.5, 130.8, 129.8, 128.0, 127.7, 127.2, 121.1, 110.6, 105.2, 63.1, 50.8, 49.7, 49.0, 43.0, 30.5, 27.6, 27.0, 22.4. HR-TOF MS. Calcd for $C_{51}H_{59}N_{10}O_{16}S_2Na_2$ ($M + Na^+$), m/z 1177.3307. Found, m/z 1177.3321.

3. Results and discussion

The bioreductive properties of 2-nitroimidazoles lead to selective cytotoxicity toward hypoxic cells within tumours [29]. Nitroimidazoles serve as hypoxic cell radiosensitizers, via a free-radical mechanism, increasing the sensitivity to radiation of normally radiation-resistant hypoxic cells [30]. Many nitroimidazole derivatives are known [31,32], and their anti-cancer applications have been studied. Misonidazole (**2**) [33], etanidazole (**3**) [34], and sanazole (**4**) [35,36] are important examples, as shown in Scheme 1.

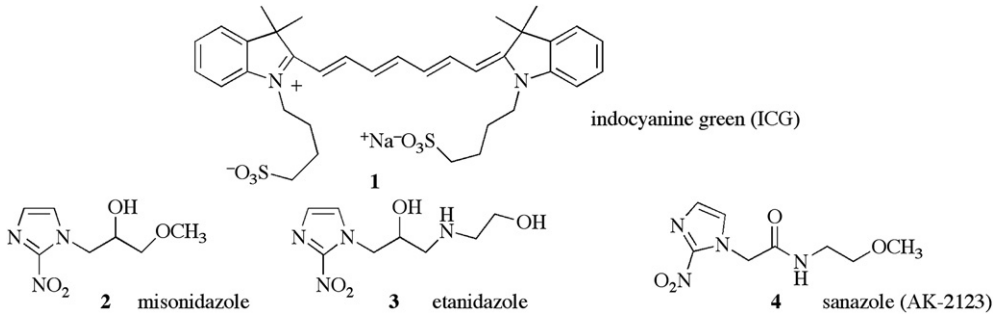

Scheme 1. ICG, misonidazole, etanidazole and sanazole.

Within the tumour, anaerobic enzymatic reduction of the nitroimidazole derivatives generates cytotoxic metabolites.

Our initial goals were to verify that (a) a nitroimidazole moiety can be incorporated into an ICG derivative and (b) verify that the new dye-conjugates retain useful fluorescent properties and stability. These studies are essential before the ultimate goal of developing a hypoxia tumour probe could be examined. We therefore chose a *bis*(carboxylic acid) derivative of ICG as the prototype dye, specifically **9**. The choice is dictated by the need to attach a nitroimidazole unit, and suggested by previous work that functionalized indocyanine carboxylic acid derivatives. It is noted that the increased fluorescence quantum yield of **9** is probably due to the observation that formation of fluorescence-quenched aggregates is suppressed because dye–dye interaction and aggregation is reduced by hydrophilic, non-charged but sterically demanding substituents [17,37].

A straightforward synthesis of **9** was reported by Lindsey and co-workers [38], in which the reaction of *p*-hydrazinobenzoic acid (**5**) with 3-methyl-2-butanone gave a 71% yield of **6**, via a Fischer indole synthesis. Subsequent treatment with butanesultone gave a 32% yield of **7**. Southwick and Grzywinski reported a modified procedure [39]. Ozinskas and co-workers prepared **6** by a similar

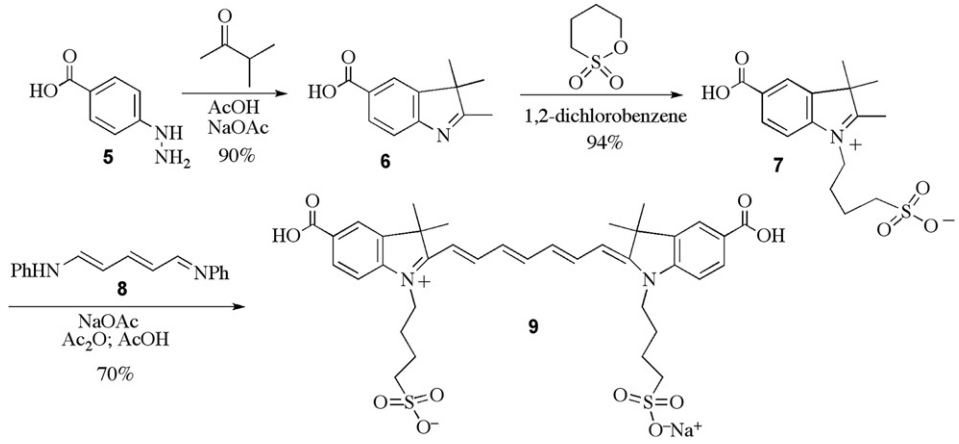

Scheme 2. Synthesis of ICG carboxylic acid derivative **9**.

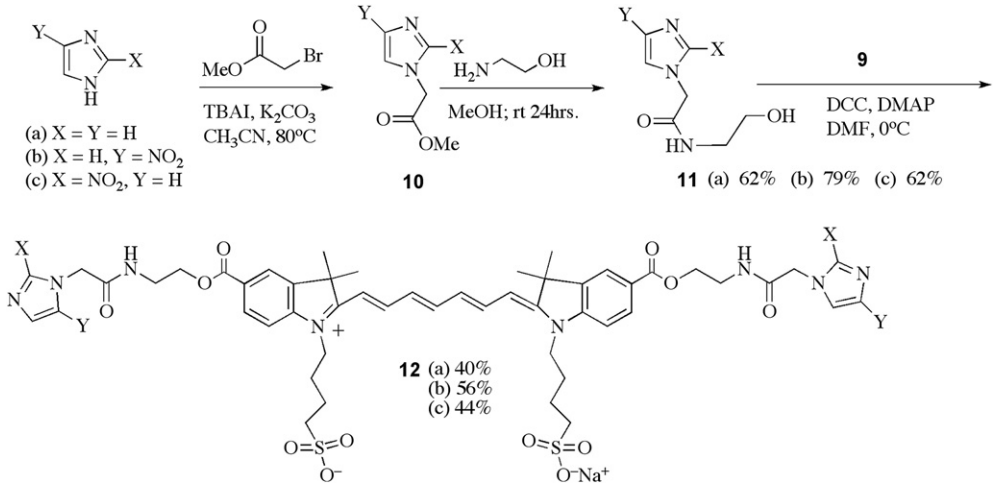

Scheme 3. Synthesis of imidazole–ICG conjugates **12**.

route, in 98% yield [20]. In this later case, treatment of **6** with ethyl iodide at 120 °C in a sealed tube gave **7** in 26% yield, and heating with butanesultone at 180 °C gave **9** in 82% yield [20]. Licha et al. prepared **9** by a similar route [17]. In all cases the dyes were assembled by condensation of **7** with the commercially available glutaconic aldehyde dianilide·HCl (**8**) [17,28,38,39]. This synthesis is shown in Scheme 2.

The targeted 2-nitroimidazole-dye conjugate combines the known compound **4** with the known compound **9**. We prepared three derivatives, however, based on conjugating the dye with imidazole, 4-nitroimidazole and 2-nitroimidazole. Initial experiments attempted to link the ethanolamine unit to the arylhydrazine **5**, but all attempts gave little or no yield of the desired compounds. The actual synthesis started with the reaction of the imidazoles and methyl bromoacetate to give the corresponding imidazole acetate, **10**. Subsequent reaction with ethanolamine would generate key intermediate **11**. Using this methodology, we prepared imidazole intermediate **10a** in 91% yield, **10b** in 89% and **10c** in 81%. Reaction of these imidazole acetate ethanolamine gave imidazole derivative **11a** in 62% yield, the 4-nitroimidazole derivative **11b** in 79% yield, and the 2-nitroimidazole derivative **11c** in 62% yield. Simple DCC coupling of the alcohol **11a–c** and **9** and the amide gave the targeted dye-conjugates **12a–c**. We prepared imidazole-dye conjugate **12a** in 40% yield, the 4-nitroimidazole-dye conjugate **12b** in 56% yield, and the 2-nitroimidazole-dye conjugate **12c** in 44% yield. The synthetic steps for the preparation of **12** are shown in Scheme 3.

4. Photophysical characterization and hypoxia evaluation

4.1. Absorption and fluorescence properties

The indocyanine green derivative **9** and imidazole conjugates **12a–c** were spectrally characterized by using an UV–Vis spectrophotometer and a fluorescence spectrophotometer (Varian Analytical Instruments, Walnut Creek, CA). The wavelength range of both spectrophotometers is 250 nm–1100 nm. The dyes were suspended in Phosphate Buffer Saline (PBS) and the absorption and fluorescence spectra were recorded. The normalized absorption and fluorescence spectra of 1 μM of **9** are shown in Fig. 1. The photophysical properties of **9** and **12a–c**, in Phosphate Buffer Saline (PBS), are shown in Table 1, with absorbance peaks at 754–756 nm and fluorescence peaks at 778–779 nm. Both **9** and **12a–c** show a blue shift of 25 nm and 30 nm in the absorption and fluorescence spectra, respectively. There is no change in absorption and fluorescence spectral profiles between **9** and **12a–c**. The extinction coefficients are 1.8 times higher than that of standard ICG, **1**. The relative quantum yields are calculated using Sigma–Aldrich's **1** as standard [17]. The relative quantum yields of the new compounds are 4.5–5.5 times higher than that of **1**. Among all the imidazole conjugates, 2-nitroimidazole ICG **12c** gives highest quantum yield. The specificity of the projected nitroimidazole imaging will depend on the oxygen concentration at which bioreductive trapping occurs, and the enzyme activity of bioreductive activation [40]. As noted earlier, nitroimidazoles are selectively reduced by nitroreductase enzymes under hypoxic conditions to form reactive products that can bind to cellular nucleophiles [2]. Because **12c** has a higher reduction potential and a highest quantum yield, it was selected for the *in-vitro* hypoxia evaluation in 4.3.

Table 1
List of optical and photophysical properties of the ICG and imidazole conjugate in PBS.

Dye	λ_{abs} (nm)	λ_{em} (nm)	Extinction Coefficient, ε (M^{-1} cm^{-1})	Quantum Yield (Φ)
ICG (Sigma–Aldrich)	779	807	11,5000	0.012
ICG	754	778	21,1000	0.066
Imidazole ICG	754	778	20,4100	0.061
2-Nitroimidazole ICG	756	779	20,5222	0.066
4-Nitroimidazole ICG	755	779	20,7519	0.054

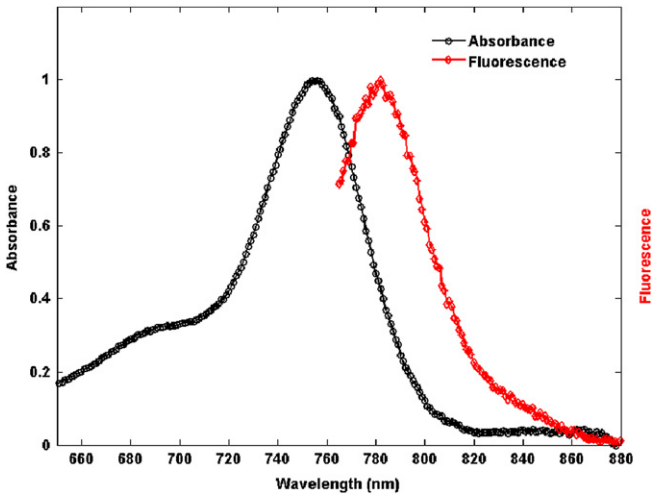

Fig. 1. Normalized absorption and fluorescence spectra of 1 μM ICG in PBS.

4.2. Optical stability of compounds

The optical stability of **12a–c** was tested in a cell culture medium, at 37 °C. The sample holder was connected to a Fisher Isotemp® Waterbath (Fisher Scientific) allowing a constant temperature to be maintained throughout the measurement. The effect of protein on molecular stability was assessed by adding **12a–c** to a cell culture medium (90% DMEM: Dulbecco's Modified Eagle Medium 1× and 10% FBS: Fetal Bovine Serum). For spectroscopic measurements, **12a–c** were suspended in a cell culture medium (90% DMEM: Dulbecco's Modified Eagle Medium 1× and 10% FBS: Fetal Bovine Serum). FBS was added to the DMEM and the dyes were kept in a spectroscopic grade cuvette for measurement at 1-h intervals, to mimic the stability of the compounds inside the

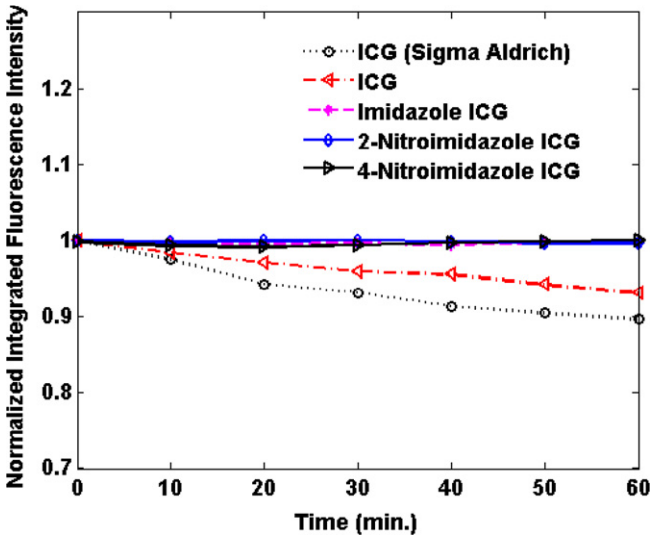

Fig. 2. Optical Stability of standard ICG, ICG carboxylic acid derivative and Imidazole conjugates in the cell culture medium at 37 °C.

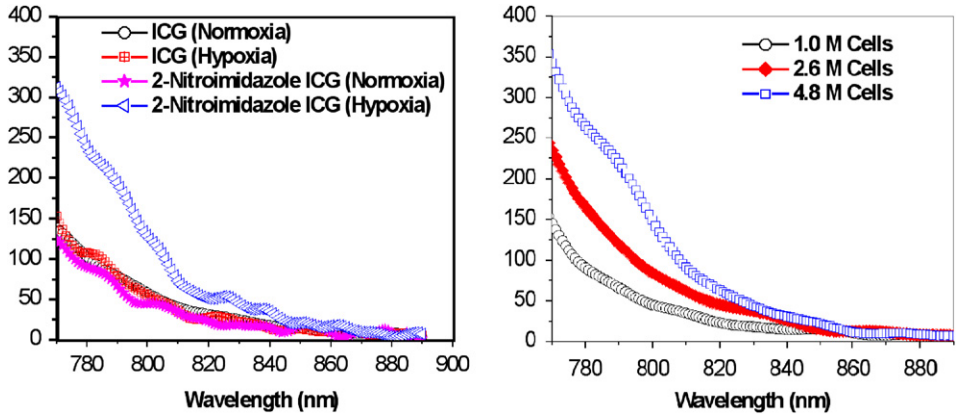

Fig. 3. (a) Fluorescence emission from 1 million cells treated with 5 μM ICG and 2-nitroimidazole ICG in hypoxia and normoxia conditions, (b) Fluorescence emission from dishes with different density of cells (M stands for millions in figure legend) at fixed 2-nitroimidazole ICG concentration of 1 μM.

body during future *in-vivo* imaging. The fluorescence spectra were collected for 60 min at intervals of 10 min. The integrated fluorescence intensities of different compounds at different incubation times are shown in Fig. 2. There was no change in the spectral profile during the 1 h measurement time, and the fluorescence intensity was diminished by 11% for **1**, 6% for **9** and less than 1% for the imidazole conjugates **12a**–**c**. These results confirm that there will be no significant bleaching or spectral fluctuations of the dye-conjugates during real-time *in-vivo* imaging, where the conjugate binding to the hypoxic cells will be the main focus.

4.3. In-vitro hypoxia evaluation

For *in-vitro* cell hypoxic studies, the 4T1 luc cells were passed 10 times in a T75 flask (BD Biosciences, Bedford, MA) prior to this study and the confluence was 70–80%. The cells were harvested and cultured in 60 × 15 mm surface-modified polystyrene tissue culture dishes (BD Falcon, Franklin Lakes, NJ, USA) 15 h prior to the dye treatment. After incubation for 15 h, the dishes were treated with 5 μM **9** and 2-nitroimidazole ICG, **12c**, and placed inside hypoxic chamber (Billups-Rothenberg, Inc., Del Mar, CA, USA). A customized mixture (95% N_2 and 5% Co_2) of gases (Airgas East, Cheshire, CT) was passed into the hypoxic chamber for 5 min and the chamber was incubated at 37 °C for 4 h [41]. The gas pressure was 2 psi throughout the 5 min passage. The dishes were washed twice in PBS, trypsinized and loaded with 2 mL of cell culture media prior to measurements. The cells were transferred to a spectroscopic grade cuvette and fluorescence measurements were done within a minute. There were around 1.5 millions of cells in each cuvette in 2 mL of media. Several measurements were done to check the consistency of our results. The fluorescence spectra of the cells treated with the **9** and with **12c** under normoxia and hypoxia conditions are shown in Fig. 3(a). The ratio of integrated fluorescence intensities of hypoxia to that of normoxia is 2.5 for **12c** treated cells and, there is no significant difference for cells reacted with **9**. This 2.5 factor for hypoxic compounds may be suitable for *in-vivo* hypoxia imaging. Testing was also done with dishes having different density of cells and all were treated with **12c** and incubated under hypoxia. This testing mimics the amount of binding to different size hypoxic tumours. The fluorescence emissions from all the three dishes are shown in Fig. 3(b) and a linear increase in fluorescence emission with cell density was observed.

5. Summary

We have successfully synthesized a new conjugate of the known ICG carboxylic acid derivative **9** and a 2-nitroimidazole moiety that is a well-known hypoxia marker. Our work generated three dye-conjugates, **12a**–**c**. The spectral characteristics of dyes **9** and **12a**–**c** are reported, including their absorption and fluorescence properties. All compounds are optically stable in protein medium, at body temperature. The quantum yields are around 5 times higher, hence higher the detection sensitivity in compared to that of cardiogreen. An *in-vitro* hypoxic evaluation has been done with 4T1 luc breast cancer cell lines. The cells treated with **12c** show 2–3 times improvement in contrast in the fluorescence signal between hypoxic and normoxic conditions. More tests will be done to validate the contrast and sensitivity of the conjugates at different concentrations of conjugates and different density of cells in both hypoxic and normoxic conditions. Our preliminary *in-vitro* data provide sufficient encouragement for continued pursuit of our hypothesis that dye-conjugate **12c** will provide the means to image tumour hypoxia in tumour-bearing mice using near-infrared techniques. The ultimate goal of this research is to develop an *in-vivo* molecular probe as well as associated imaging hardware that can directly image tumour hypoxia of breast cancer patients who may be resistant to traditional therapies and can benefit from hypoxia-targeted therapies. Based on this preliminary work, future studies will involve *in-vivo* hypoxic testing with mice having tumours at the mammary pad. The hypoxia will be evaluated at different stages of tumour growth.

References

[1] Hockel M, Vaupel P. Tumour hypoxia: definitions and current clinical, biologic, and molecular aspects. Journal of the National Cancer Institute 2001; 93:266–76.
[2] Kizaka-Kondoh S, Inoue M, Harada H, Hiraoka M. Tumour hypoxia: a target for selective cancer therapy. Cancer Science 2003;94:1021–8.
[3] Krohn KA, Link JM, Mason RP. Molecular imaging of hypoxia. Journal of Nuclear Medicine 2008;49:129S–48S.
[4] Hockel M, Schlenger K, Knoop C, Vaupel P. Oxygenation of carcinomas of the uterine cervix: evaluation by computerized O_2 tension measurements. Cancer Research 1991;51:6098–102.
[5] Brizel DM, Sibley GS, Prosnitz LR, Scher RL, Dewhirst MW. Tumour hypoxia adversely affects the prognosis of carcinoma of the head and neck. International Journal of Radiation Biology and Related Studies in Physics 1997;38:285–9.
[6] Hilderbrand SA, Weissleder R. Near-infrared fluorescence: application to in vivo molecular imaging. Current Opinion in Chemical Biology 2010;14:71–9.
[7] Hamer FM. Cyanine dyes. Quarterly Reviews (London) 1950;4:327–55.
[8] Sturmer DM. Synthesis and properties of cyanine and related dyes. In: Weissberger A, Taylor E, editors. Special topics in heterocyclic chemistry. New York: Wiley; 1977. p. 441.
[9] Venkataraman K. The chemistry of synthetic dyes, vol. 2. New York: Academic Press; 1952. p. 1143.
[10] Hamer FM. The cyanine dyes and related compounds. New York: Wiley; 1964.
[11] Fox IJ, Wood EH. Indocyanine green: physical and physiologic properties. Proceedings of the Mayo Clinic 1960;35:732–44.

[12] Ogawa M, Kosaka N, Choyke PL, Hisataka Kobayashi H. In vivo molecular imaging of cancer with a quenching near-infrared fluorescent probe using conjugates of monoclonal antibodies and indocyanine green. Cancer Research 2009;69:1268–72.
[13] Landsman ML, Kwant G, Mook GA, Zijistra WG. Light-absorbing properties, stability, and spectral stabilization of indocyanine green. Journal of Applied Physiology 1976;40:575–83.
[14] Ishizawa T, Fukushima N, Shibahara J, Masuda K, Tamura S, Aoki T, et al. Real-time identification of liver cancers by using indocyanine green fluorescent imaging. Cancer 2009;115:2491–504.
[15] Ishizawa T, Bandai Y, Harada1 N, Muraoka1 A, Ijichi M, Kusaka K, et al. Indocyanine green-fluorescent imaging of hepatocellular carcinoma during laparoscopic hepatectomy: an initial experience. Asian Journal of Endoscopic Surgery 2010;3:42–5.
[16] Kusanoa M, Tajimaa Y, Yamazakia K, Katoa M, Watanabea M, Mitsuharu M. Sentinel node mapping guided by indocyanine green fluorescence imaging: a new method for sentinel node navigation surgery in gastrointestinal cancer. Digestive Surgery 2008;25:103–8.
[17] Licha K, Riefke B, Ntziachristos V, Becker A, Chance B, Semmler W. Hydrophilic cyanine dyes as contrast agents for near-infrared tumour imaging: synthesis, photophysical properties and spectroscopic *in vivo* characterization. Photochemistry and Photobiology 2000;72:392–8.
[18] Vaupel P, Kallinowski F, Okunieff P. Blood flow, oxygen and nutrient supply, and metabolic microenvironment of human tumours: a review. Cancer Research 1989;49:6449–65.
[19] Padhani AR. Where are we with imaging oxygenation in human tumours? Cancer Imaging 2005;5:128–30.
[20] Terpetschning E, Szmacinski H, Ozinskas A, Lakowicz JR. Synthesis of squaraine-N-hydroxysuccinimide esters and their biological application as long-wavelength fluorescent labels. Analytical Biochemistry 1994;217:197–204.
[21] Sanders JM, Gomez AO, Mao J, Meints GA, van Brussel EM, Brzynska A, et al. 3-D QSAR investigations of the inhibition of leishmania major farnesyl pyrophosphate synthase by bisphosphonates. Journal of Medicinal Chemistry 2003;46:5171–83.
[22] Pellicciari R, Curini M, Spagnoli N, Ceccherelli P. Reactions of alkoxycarbonylcarbenoids with imidazole: an improved preparation of ethyl imidazole-1-ylacetate and the first synthesis of diethyl imidazole-1-ylmalonate. Synthesis; 1981:629–31.
[23] Avery M, Estela M, Maris E, Williamson J. Design and synthesis of heterocyclic hydroxamic acid derivatives as inhibitors or helicobacter pylori urease. Synthetic Communications 2003;33:1977–95.
[24] Long A, Parrick J, Hodgkiss RJ. An efficient procedure for the 1-alkylation of 2-nitroimidazoles and the synthesis of a probe for hypoxia in solid tumours. Synthesis; 1991:709–13.
[25] Kasai S, Nagasawa H, Yamashita M, Masui M, Kuwasaka H, Oshodani T, et al. New antimetastatic hypoxic cell radiosensitizers: design, synthesis, and biological activities of 2-nitroimidazole-acetamide, TX-1877, and its analogues. Bioorganic and Medicinal Chemistry; 2001:453–64.
[26] For a general procedure for coupling ethanolamine, see Fong MT, Leaffer MA. Synthesis of 1-(2,3-dihydroxypropyl)-2-nitro-1H-imidazole-2-14C and N-(2-hydroxyethyl)-2-(2-nitro-1-H-imidazol-1-yl-2-14C)acetamide. Journal of Labelled Compounds and Radiopharmaceuticals 1986;23:981–5.
[27] Lee WW, Brown JM, Martinez AP, Cory MJ. Nitroimidazoles of low toxicity and high activity as radiosensitizers of hypoxic tumour cells. US Patent 4371540 1983.
[28] Neises B, Steglich W. Esterification of carboxylic acid with DCC/DMAP: tert-Butyl ethyl fumarate. Organic Syntheses 1990;Collective vol. 7:93–5.
[29] Gielen AP, Sartorelli AC, editors. Collected papers in biochemical pharmacology, vol. 35. Oxford (UK): Pergamon Press; 1986. p. 1–122.
[30] Adams GE, Michael BD, Asquith JC, Shenoy MA, Watts ME, Whillans DW. Radiation research: biomedical, chemical and physical perspectives. New York: Academic Press; 1975. p. 92–478.
[31] Jenkins TC, Naylor MA, O'Neill P, Threadgill MD, Cole S, Stratford IJ, et al. Synthesis and evaluation of α-[[(2-haloethyl)amino]methyl]-2-nitro-1H-imidazole-1-ethanols as prodrugs of α-[(1-aziridinyl)methyl]-2-nitro-1H-imidazole-1-ethanol (RSU-1069) and its analogs which are radiosensitizers and bioreductively activated cytotoxins. Journal of Medicinal Chemistry 1990;33:2603–10.
[32] Khlebnikov A, Scheptkin I, Kwon BS. Modeling of the anticancer action for radical derivatives of nitroazoles: quantitative structure-activity relationship (QSAR) study. Cancer Biotherapy and Radiopharmaceuticals 2002;17:193–203.
[33] Asquith JC, Watts ME, Patel K, Smithen CE, Adams GE. Electron affinic sensitization. V. Radiosensitization of hypoxic bacteria and mammalian cells in vitro by some nitroimidazoles and nitropyrazoles. Radiation Research 1974;60:108–18.
[34] Brown JM, Yu NY, Brown DM, Lee W. SR-2508: a 2-nitroimidazole amide which should be superior to misonidazole as a radiosensitizer for clinical use. International Journal of Radiation Biology and Related Studies in Physics 1981;7:695–703.
[35] Kondakova IV, Tcheredova VV, Zagrebelnaya GV, Cherdyntseva NV, Kagiya TV, Choinzonov EL. Production of nitric oxide by hypoxic radiosensitizer sanazole. Experimental Oncology 2004;26:331–3.
[36] Shibamoto Y, Sakano K, Kimura R, Nishimoto SI, Ono K, Kagiya T, et al. Radiosensitization in vitro and in vivo by 3-nitrotriazoles. International Journal of Radiation Oncology, Biology, Physics 1986;12:1063–6.
[37] Mujumdar SR, Mujumdar RB, Grant CM, Waggoner AS. Cyanine-labeling reagents: sulfobenzindocyanine succinimidyl esters. Bioconjugate Chemistry 1996;7:356–62.
[38] Lindsey JS, Brown PA, Siesel DA. Visible light-harvesting in covalently-linked porphyrin-cyanine dyes. Tetrahedron 1989;45:4845–66.
[39] Southwick PL, Grzywinski MP. 1988. Unpublished work. Citation 41 in reference [32] (T-89-p4845).
[40] Kizaka-Kondoh S, Konse-Nagasawa H. Significance of nitroimidazole compounds and hypoxia-inducible factor-1 for imaging tumour hypoxia. Cancer Science 2009;1:1–7.
[41] Allen CB, Schneider BK, White CW. Limitations to oxygen diffusion and equilibration in vitro cell exposure systems in hyperoxia and hypoxia. American Journal of Physiology – Lung Cellular and Molecular Biology 2001;281:L1021–7.